Research Article

Journal of Molecular Recognition

Received: 23 January 2009, Revised: 27 June 2009, Accepted: 30 June 2009, Published online in Wiley InterScience: 29 July 2009

(www.interscience.wiley.com) DOI:10.1002/jmr.975

A Combined Atomic Force Microscopy Imaging and Docking Study to Investigate the Complex Between p53 DNA Binding Domain and Azurin

Anna Rita Bizzarri[a]*, Silvia Di Agostino[b], Laura Andolfi[a] and Salvatore Cannistraro[a]

The tumor suppressor p53 interacts with the redox copper protein Azurin (AZ) forming a complex which is of some relevance in biomedicine and cancer therapy. To obtain information on the spatial organization of this complex when it is immobilized on a substrate, we have used tapping mode-atomic force microscopy (TM-AFM) imaging combined with computational docking. The vertical dimension and the bearing volume of the DNA binding domain (DBD) of p53, anchored to functionalized gold substrate through exposed lysine residues, alone and after deposing AZ, have been measured by TM-AFM. By a computational docking approach, a three-dimensional model for the DBD of p53, before and after addition of AZ, have been predicted. Then we have calculated the possible arrangements of these biomolecular systems on gold substrate by finding a good agreement with the related experimental distribution of the height. The potentiality of the approach combining TM-AFM imaging and computational docking for the study of biomolecular complexes immobilized on substrates is briefly discussed. Copyright © 2009 John Wiley & Sons, Ltd.

Keywords: p53; Azurin; atomic force microscopy; docking; molecular dynamics simulation

INTRODUCTION

Atomic force microscopy (AFM) belongs to a wide family of nanoscopic techniques which have opened new routes to the study of the structural and functional properties of biological systems. AFM allows to image biological samples adsorbed onto a substrate (glass, mica, gold, etc.), even in physiological conditions and without any label or sample treatments, elucidating their morphological properties (Hoerber and Miles, 2003). AFM imaging is performed by scanning a very sharp tip, located at the end of a cantilever spring, over the sample surface mounted on a piezoelectric scanner which is able to assure a three-dimensional positioning with subnanometer resolution. The interaction forces between tip and sample (such as electrostatic, van der Waals, frictional, capillary, and chemical forces) are measured by the cantilever deflection which is used to create a topographical image of the sample when the tip is raster-scanned in the horizontal *x*–*y* plane. The resolution in the vertical direction is tenths of angstrom, and it is limited by thermal noise, while the resolution in the *x*–*y* plane is generally a few nanometers, being generally limited by the tip curvature radius (Butt *et al*., 2005). AFM equipment can be also used to probe intra- and inter-molecular forces in biological systems in the modality called atomic force spectroscopy (AFS). In particular, the unbinding forces and the dissociation rate of a ligand-receptor pair can be measured by recording force-versus-distance curves on a surface-bound receptor by an AFM tip functionalized with the ligand undergoing a biorecognition event (Jena and Hoerner 2002; Bonanni *et al*., 2005).

AFM imaging may also offer an alternative method to probe biorecognition events by evaluating the changes in the height and/or in the volume of imaged spots upon addition of a ligand to the receptor (Bergkvist *et al*., 2001; Bayburt and Sligar, 2002). Such an approach, which couples fast and rather simple operative way with a high sensitivity, deserves high potentialities in bio-nanomedicine to perform high throughput drug screening (Kim, 2007; Nie *et al*., 2007; Sengupta and Sasisekharan, 2007). Indeed, the most recent generation of high-speed AFM permits the recording of dynamic biological processes in real time (Schitter *et al*., 2004; Stolz *et al*., 2007).

However, a restricted knowledge of the biological system, at molecular level, might limit the AFM capabilities. In this respect, the combination of AFM with a theoretical investigation could be extremely fruitful in the refining of experimental data to clarify ambiguous aspects. For example, steered molecular dynamics simulation can help in the analysis of AFS data by providing information on the analyzed at atomic scale (Rief and Grubmueller, 2002).

Similarly, the morphological characterization by AFM imaging of complexes immobilized on a substrate, could also take a large advantage of suitable computational procedures (Davis and Hill,

* *Correspondence to: A. R. Bizzarri, Biophysics & Nanoscience Centre, CNISM, Facolta' di Scienze, Università della Tuscia, I-01100 Viterbo, Italy. E-mail: bizzarri@unitus.it*

a *A. R. Bizzarri, L. Andolfi, S. Cannistraro*
Biophysics & Nanoscience Centre, CNISM, Facolta' di Scienze, Università della Tuscia, I-01100 Viterbo, Italy

b *S. Di Agostino*
Molecular Oncogenesis Laboratory, Experimental Oncology Department, Regina Elena Cancer Institute, Via delle Messi D'oro 156, 00158 Rome, Italy

Journal of Molecular Recognition

2002; Zhao *et al*., 2004). In particular, docking algorithms, which are able to predict the three-dimensional architecture of an unknown biomolecular complex, starting from the independently solved X-ray structures of the single components, are suitable tools (Vajda and Camacho, 2004). Upon prediction of a biomolecular complex structure, its topological parameters (such as the height and volume) can be obtained.

On such a basis, we intend to exploit the capabilities of an approach combining AFM imaging and computational docking to investigate the formation of a complex between two biomolecules. Such an approach offers the possibility to elucidate the spatial organization of a complex when one of the two partners is immobilized onto a surface. Furthermore, it could allow to explore the potentialities of AFM imaging for ultrasensitive detection.

We have focused our attention to a complex between a domain of the tumor suppressor p53 and the copper redox proteins Azurin (AZ). p53 is a multi-domain protein which acts as a guardian of the genome in preventing cancer growth and maintaining genomic stability (Levine, 1997; Vogelstein *et al*., 2000; Vajda and Camacho, 2004; Di Agostino *et al*., 2006; Joerger *et al*., 2006). AZ was found to enter some mammalian cancer cells and induce apoptosis forming a complex with p53 and stabilizing it. Therefore, AZ is a very attractive candidate for developing novel anticancer strategies (Yamada *et al*., 2002, 2004; Goto *et al*., 2003) and recently, we have studied by AFS the interaction force and dissociation rate of whole p53 and AZ (Taranta *et al*., 2008).

Here, we investigate the spatial organization of the complex between AZ and the DNA binding domain (DBD) of p53 fused to glutathione *S*-transferase (GST) (for simplicity from here on we will refer to it as DBD) when immobilized onto functionalized gold. GST is a fusion protein very commonly used for synthesis of recombinant proteins in bacteria. The formation of the complex between p53 and AZ has been demonstrated to be not altered by the presence of GST (Yamada *et al*., 2004). By a TM-AFM imaging analysis, we have evaluated the height distribution of DBD biomolecules anchored on functionalized gold, before and after its interaction with AZ. In addition, the single imaged spots, corresponding to biomolecules have been analyzed by a bearing volume analysis which allows to estimate the apparent volume of the spots. Such a procedure has been applied to extract the change in the volume of DBD upon adding AZ. Since both the number and the possible regions of the interaction sites between DBD and AZ are unknown, we have applied a computational docking to provide some information on the organization of the complex by predicting the three-dimensional structure for DBD conjugated to AZ, starting from the X-ray-resolved structures for DBD and AZ. These docking procedures have taken advantage from some information on possible interacting regions between DBD and AZ (Yamada *et al*., 2004; De Grandis *et al*., 2007).

Furthermore, we have calculated the possible arrangements and the height of this biomolecular system over functionalized gold substrate, together with its volume distribution, by taking into account the accessibility of the available lysine residues. These theoretical distributions have been compared with the experimental ones. The found good agreement between these two distributions has led us to support the formation of a complex between DBD and AZ.

Generally, the approach which combines TM-AFM imaging and computational docking appears then to be a suitable method to more deeply characterize the topological features of a biomolecular system immobilized over a substrate. Furthermore, it could also have high potentialities in nanomedicine and diagnostics for detecting the formation of complexes and for screening of protein–drug interactions.

METHODS

Molecular systems

Initial coordinates of the domain DBD of p53 were taken from the chain B of PDB entry 1TUP, providing a 2.2 Å resolution crystal structure in complex with a consensus DNA binding site (Cho *et al*., 1994). The DBD consists of a β-sandwich formed by two antiparallel β-sheets (see Figure 1A). A zinc ion is tetrahedrally coordinated by S^{γ} of Cys 176, Cys 238, and Cys 242, and N^{δ} of His 179, forming a Cys_3His zinc-finger motif (Duan and Nilsson, 2006).

Initial coordinates of the fusion protein GST were taken from X-ray structure at 2.1 Å resolution (chain A of PDF entry 1A0F) (Nishida *et al*., 1998). GST has 201 amino acid residues organized by a N-terminal domain (residues 1–80), formed by a four-stranded β-sheet and two α-helices, and the larger C-terminal domain (residues 89–201) constructed by a right-handed bundle of four α-helices (see Figure 1B).

Initial atomic coordinates of AZ were taken from the X-ray structure at 1.93 Å resolution (chain B of PDB entry 4AZU) (Nar *et al*., 1991). The protein consists of an α-helix (H) and eight β-strands that form two sheets arranged in a Greek key motif. The copper active site is at the top, or northern end, of protein, about 7 Å below the surface and surrounded by a cluster of hydrophobic residues, known as the hydrophobic patch (van de Kamp *et al*., 1990). The copper ion is coordinated by three strong equatorial ligands and two weaker axial ligands. Opposite to the copper site, a disulfide bridge connecting residues Cys 3 and Cys 26 is located in the southern region of the protein (see Figure 1C) (Bonander *et al*., 2000); such a bridge contributing to the high stability of AZ (Bonander *et al*., 2000).

Protein docking

Zdock method is a rigid-body docking algorithm using a fast Fourier transform (FFT) to perform an exhaustive six-dimensional search in the translational and rotational space between the two molecules (Chen and Weng, 2002, 2003). Each protein is projected into a three-dimensional grid and different values are assigned to the cells of the grid, representing the surface or the interior of the molecules. Zdock searches orientational space by rotating the ligand around its geometric center with the receptor protein kept fixed in space. For each sampled angle, only the ligand translation corresponding to the best geometric match between the two proteins is retained. The obtained configurations for the complex are ranked on a scoring function combining shape complementarity, desolvation energy, and electrostatics. The metal ions belonging to the protein structures (copper in AZ and zinc in DBD) were included during the docking. Docking samplings were carried out by employing a $128 \times 128 \times 128$ point grid with a spacing of 1.2 Å and a rotational interval of 6°. In all the simulations, one molecule was kept fixed and the other one was allowed to rotate and translate in order to explore the whole conformational space of the complex. In the first docking step, DBD was kept fixed and GST was allowed to rotate and translate, while in the second step, GST-DBD was kept fixed and AZ was allowed to rotate and translate.

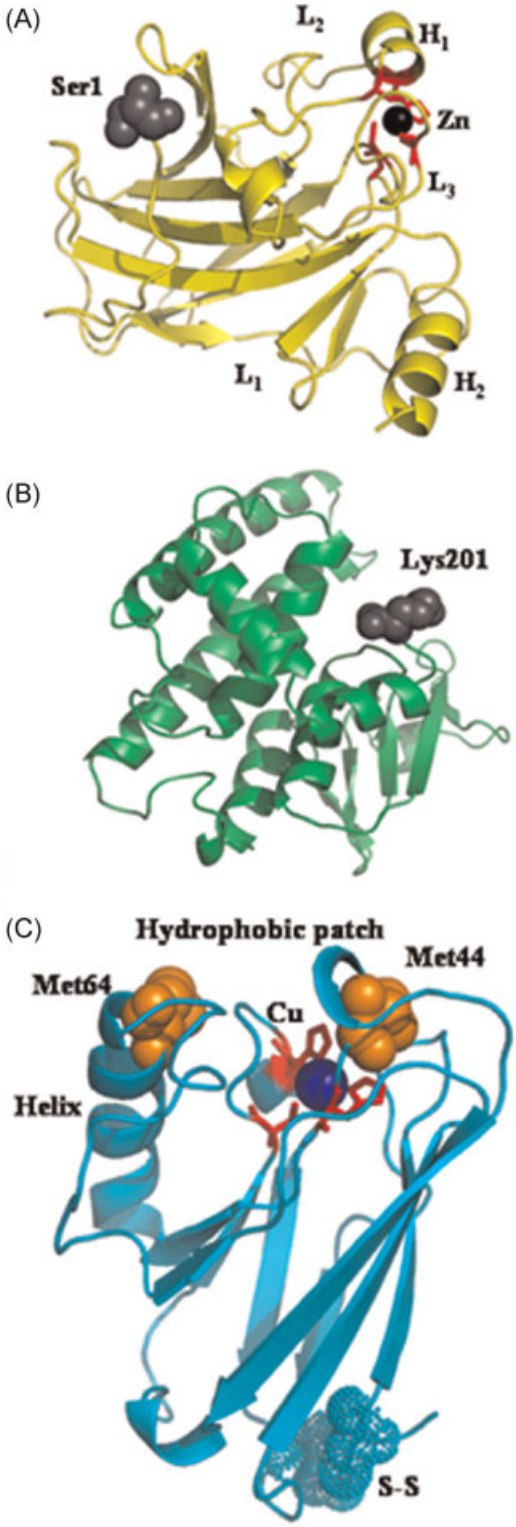

Figure 1. Three-dimensional representation of the crystallographic structure of: (A) DBD domain of p53; (B) GST; and (C) AZ.

The top 2000 outcomes predicted by Zdock for the complex were preliminarily grouped in clusters in order to eliminate very similar conformations. Indeed, the largest part of predicted complexes differ among them only for very few structural details. Such a cluster analysis was performed by using the ClusPro docking server by using a pairwise binding site root mean squared deviation (RMSD) criterion. In particular, complexes whose structures differ between them for an RMSD value less than a clustering radius were put in the same group; the clustering radius being set to $R_c = 8$ Å (Comeau *et al.*, 2004). The top clusters generated by ClusPro were retained for further analysis.

Molecular dynamics simulations

MD simulations were performed with the GROMACS 3.2.1 package, using the GROMOS96 43a1 force field (van der Spoel *et al.*, 2001). Each biomolecule was solvated in an SPC water box (Berendsen *et al.*, 1969) extending to at least 6 Å from the complex surface.

AZ active site was modeled by applying bond-stretching and bond-bending harmonic potentials between the copper ion and the nitrogen atoms of His 46 and His 117 and the sulfur atom of Cys 112, while the interactions of copper with the thioether sulfur of Met 121 and the carbonyl oxygen of Gly 45 were treated by a non-bonded approach (Bizzarri *et al.*, 2007; De Grandis *et al.*, 2007).

The zinc-finger topology in the p53 DBD was described through a bonded approach, according to Calumet and Simonson (2006). Zinc was covalently bound to four ligands: three sulfur atoms from Cys 176, Cys 238, and Cys 242 and one nitrogen from His 179 (Maynard and Covell, 2001; De Grandis *et al.*, 2007). Counterions were added to the simulation box to keep the simulated systems neutral. The MD simulations were carried out in the NPT ensemble with $T = 300$ K and $P = 1$ bar. The Nose–Hoover thermostat method was used to control the system temperature, with coupling time constant $\tau_T = 0.1$ ps (Nose', 1984). Constant pressure was imposed using the Parrinello–Rahman extended-ensemble ($\tau_P = 1.0$ ps) (Parrinello and Rahman, 1981). The long-range electrostatics were treated with the particle mesh Ewald (PME) method with a lattice spacing of 1.2 Å. A 9 Å cut-off was employed for Lennard–Jones interactions (Kholmurodov *et al.*, 2000). The pair list was updated every 10 MD steps. All covalent bonds were constrained with the LINCS algorithm (Hess *et al.*, 1997). The time step was chosen to be 2 fs. The complexes were minimized with steepest descent and gradually heated from 50 to 300 K at 20 ps increments of 50 K. The systems were then equilibrated by a 600 ps MD simulation under position restraints. Finally an unrestrained MD run was carried out for 3 ns. The first 2 ns of the run were treated as a further equilibration simulation and the remainder 1 ns was taken for data collection.

Sample preparation

The DBD domain of p53 bound to GST and GST proteins (solubilized in 1.23 μM in 50 mM Tris–acetate, pH 7.5, 1 mM EDTA, 20% glycerol) were prepared as following. *E. coli* BL21DE3 (pSpsA) strain transformed with pGEX-4X-DBD-p53 and pGEX-4X constructs were grown at 30°C in LB medium to an optical density (OD 600 nm) of 0.4. Expression of recombinant proteins was induced by the addition of 1 mM isopropyl-1-thio-β-galactopyranoside for over night at room temperature under constant shaking. Cells were pelleted and lysed in 1X phosphate-buffered saline (PBS) containing 0.1% Triton X-100, 1 mM DTT, protease inhibitors, by probe sonication (three cycles of 1 min each). Bacterial extracts were clarified by centrifugation and supernatant fractions were incubated with glutathione-Sepharose

Journal of Molecular Recognition

beads (Sigma, G 4510) for 2 h at 4°C with constant shaking. After several washes in 1X PBS, proteins were eluted with 50 mM Tris–HCl pH 8, containing 10 mM glutathione (Sigma, G 4251) and 1 mM DTT.

AZ (20 μM in PBS) from *Pseudomonas aeruginosa* (14.6 kDa) was purchased from Sigma and dissolved in PBS buffer (50 mM at pH 7).

The gold substrates (from Arrandee) consist of vacuum-evaporated thin gold films (thickness 250 nm) on borosilicate glass. The gold-glass substrates were flame-annealed, to obtain atomically flat Au(111) terraces over hundreds of nanometers, with a typical roughness R_q of 0.18 ± 0.09 nm, as determined by AFM.

To prepare the functionalized gold sample, the gold substrate was incubated with a 0.2 mM cysteamine solution for 4 h at room temperature to form a monolayer, bound to gold through thiol groups, and exposing amino groups. Subsequently, the substrate was reacted with 0.2 mM glutaraldehyde at room temperature and then rinsed with milliQ water. This functionalized substrate was incubated for 2 h with 80 μl solution of 125 ng/ml GST-DBD and successively, with 100 μl of 20 μM AZ solution for 4 h at room temperature.

AFM imaging and analysis

A Nanoscope IIIa/Multimode AFM (Veeco Instruments, Santa Barbara, CA) was used to image samples in milliQ water. We verified that the corresponding images presented the same features of those performed in buffer, provided that the pH was adjusted at the same value. All measurements were done in Tapping Mode AFM (TM-AFM), using silicon tips (Veeco Instruments) with a nominal radius less than 10 nm and a nominal spring constant of 0.5 N/m, operating at a resonance frequency of about 100 kHz and at an amplitude set point to the 95% of the free amplitude value. An estimation of the effective tip radius was performed according to Bonanni and Cannistraro (2005). Such a procedure allowed also to estimate the vertical resolution, which was found to be around 0.2 nm. TM-AFM images of 500×500 nm^2 scan size were recorded. Analysis of the AFM images was performed using the analysis tools of the nanoscope software and the WSxM software (Horcas *et al*., 2007). The bearing volume analysis was carried out by the Veeco software (Nanoscope 5.12r5) on raw AFM images. For each spot the bearing volume was measured from the top to the 80% of the total height.

Figure preparation

Figures were created with Pymol (Guex and Peitsch, 1997).

RESULTS AND DISCUSSION

AFM imaging experiments

An analysis of the TM-AFM images of gold substrates functionalized with glutaraldehyde and cysteamine reveals the presence of rather regular spots uniformly distributed over the surface with a height between 1 and 2 nm (see Figure 2A). The roughness of the surfaces, R_q, obtained by averaging over 20 different regions with area of 200×200 nm^2 is 0.52 ± 0.08 nm. These features are in a very good agreement with those reported in literature for the same kind of samples (Ferreira *et al*., 2006). Upon incubating this functionalized gold substrate with a solution containing DBD for 2 h and rinsing with milliQ water, bright large spots randomly distributed over the surface appear in the TM-AFM images recorded in milliQ water (see Figure 2B). These spots are well distinct from those observed in the functionalized substrate and they are characterized by a mean height exceeding 4 nm (see a representative section analysis in Figure 2B). The number of large spots has been observed to increase with the incubation time and eventually reaching an almost complete coverage. The TM-AFM images of the DBD

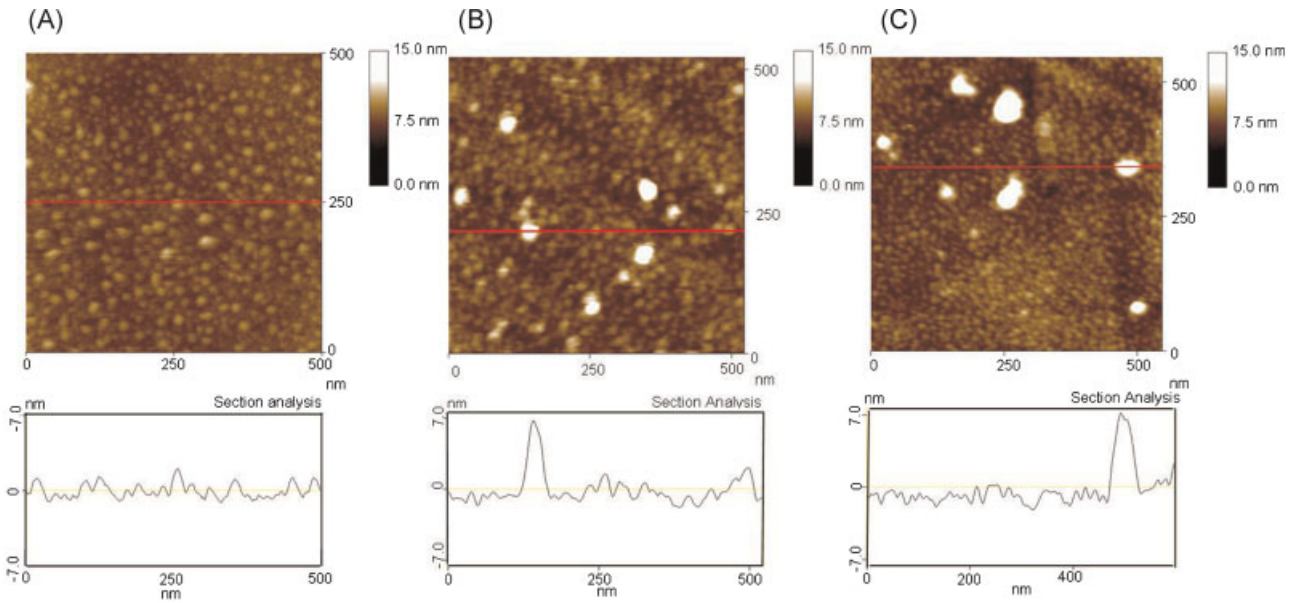

Figure 2. TM-AFM image and section analysis of: (A) functionalized substrate obtained by glutaraldehyde–cysteamine monolayer assembled on Au(111) surface; (B) DBD deposited over the functionalized substrate; (C) DBD-AZ deposited over the functionalized substrate. All the images have been acquired in milliQ water.

samples have been found to be stable under repeated scans, indicating that the biomolecules are firmly anchored to the substrate. This is consistent with the covalent attachment of DBD biomolecules to the functionalized gold substrate, likely through lysine residues (Bonanni *et al*., 2007). Then, we have performed a cross-section analysis on 100 individual spots. The histogram of these heights with a binning set at 0.5 nm by taking into account the vertical resolution and the biomolecular size of about 3–4 nm is shown in Figure 3A. The histogram reveals a single mode distribution with an average value of 6.4 nm and a standard deviation of 1.9 nm. This distribution can be well described by a Gaussian as checked by the χ^2-test (see continuous curve in Figure 3A and the related legend). The central value finds a correspondence with the dimension of DBD fused to GST (see also below). In this respect, we mention that the slight load applied by the AFM tip on the protein sample does not appear to significantly affect the vertical dimension of the proteins; the occurrence of some reduction on the height could be masked by the contribution to the distributions from other effects.

The observed spread in the height values of the biomolecules, as detected by TM-AFM, can be put into relationship to a scattered arrangement of the biomolecules with respect to the gold substrate; this being likely due to a heterogeneity in the attachment points (lysine residues) of the biomolecule on the substrate.

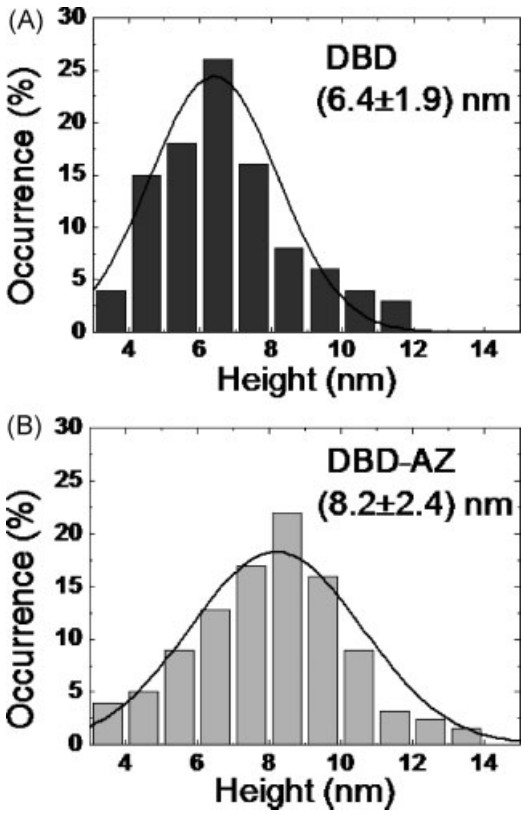

Figure 3. Histograms of the height from 100 individual cross-section analysis from TM-AFM images for: (A) DBD deposited over the functionalized substrate; (B) DBD-AZ DBD deposited over the functionalized substrate. Continuous lines: best-fit by a Gaussian distribution. The agreement between the histogram and the fitted Gaussian distribution has been checked by a χ^2-test at the confidence level of 90%.

Figure 2C shows an example of the TM-AFM images obtained from the DBD sample, upon incubation with a solution containing AZ, and rinsing with milliQ water. Again, bright spots, randomly distributed over the surface, can be clearly seen. The TM-AFM images of the DBD-AZ samples have been found to be stable under repeated scans. Again a cross section analysis from 100 imaged spots has been carried out. The related histogram, with the binning of 0.5 nm, exhibits a single mode distribution characterized by a central value, 8.2 nm, and by a standard deviation of 2.4 nm (see Figure 3B). This distribution can be well described by a Gaussian (see Figure 3B and the related legend). A shift of the height histograms toward higher values is detected upon adding AZ. Such a shift is consistent with a change of the topological properties of the sample, as verified by a *t*-test at the confidence level of 90% (Spieger, 1961). Notably, a control experiment performed by anchoring GST alone on functionalized gold substrate, followed by the addition of AZ and successively a rinsing with milliQ water, has revealed that practically no change in the height distribution takes place (not shown); this being in agreement with the observation that GST and AZ do not give rise to a specific interaction (Yamada *et al*., 2002).

As further control, we have also performed an experiment in which AZ has been deposited on the functionalized gold substrate. The histogram of the height, with the binning of 0.5 nm, exhibits again a single mode distribution with a central value of 3.6 nm, and with a standard deviation of 1.6 nm (not shown). These data are in a very good agreement with those obtained in our previous works in which AZ was immobilized on gold functionalized by a sulfhydryl-terminated spacer (Bonanni *et al*., 2006).

Further information on the arrangement of the complex on the substrate has been obtained by performing a bearing volume analysis. Figure 4 shows the histograms of the bearing volume, as evaluated from the same 100 spots previously analyzed. Some spread in the bearing volume has been observed for both DBD and DBD-AZ samples. The average value for the DBD-AZ is peaked at a slight higher value in comparison to that of the DBD sample. In particular, the bearing volume passes from 1.4×10^4 nm^3 for DBD to 1.9×10^4 nm^3 for DBD-AZ. However, the extracted distributions do not allow us to reach a definitive conclusion about the formation of a complex between DBD and AZ. On the other hand, we remark that the extracted values do not represent real volumes of the imaged molecules, since the tip

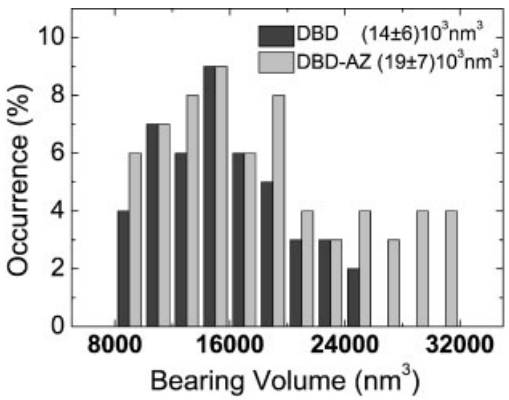

Figure 4. Histograms of the bearing volume measured from the top to the 80% of the total height from 100 individual spots from the TM-AFM images for DBD and DBD-AZ samples.

Journal of Molecular Recognition

convolution effect significantly affects the lateral dimension of the protein, yielding a large overestimation of the bearing volume.

To get a stronger evidence on the formation of a complex between DBD and AZ, the expected heights and bearing volumes of the biomolecules when immobilized on functionalized gold surface through the exposed lysines should be evaluated. With such an aim, we have followed a docking computational approach which, first predicts the structures of the expected complexes, and then it allows to extract the corresponding height over the substrate by taking into account the binding through the different available lysines on the surface.

Docking between GST and DBD and between GST-DBD and AZ

The arrangement of a biomolecular system immobilized on a substrate could be in principle predicted if its three-dimensional structure is known (Bizzarri *et al*., 2003; Bizzarri, 2006). However, since the crystallographic structure of our complexes is not available, we have applied a suitable docking procedure to extract the three-dimensional structure of the best possible complex.

Our docking procedure consists of two steps. First, we have performed a docking between DBD and GST. The results of this step has been the starting point for the second step searching the best complex between DBD and AZ, by also exploiting the results from the docking between the DBD domain of p53 and AZ (De Grandis *et al*., 2007).

The first step is rather simple, since the presence of a covalent bond between the N-terminal (Ser1) of DBD and the C-terminal (Lys201) of GST drastically restricts the number of possible configurations for the complex between DBD and GST. The top 2000 complexes between DBD and GST, predicted by Zdock, have been preliminarily filtered by requiring that the distance between the C-terminal (Lys201) of GST and the N-terminal (Ser1) of DBD was within 0.15 nm in order to match the formation of a covalent bond between these two atoms. Furthermore, it has been required that the DNA binding region of the DBD chain is left exposed, as experimentally required (Yamada *et al*., 2002). The resulting models have been then grouped by ClusPro clustering scheme generating five candidates for the DBD; the highest ranked model in each group being retained for further analysis. At visual inspection, the selected complexes are clustered together at the opposite region where the DNA binding site is located with rather similar structures (not shown). All these

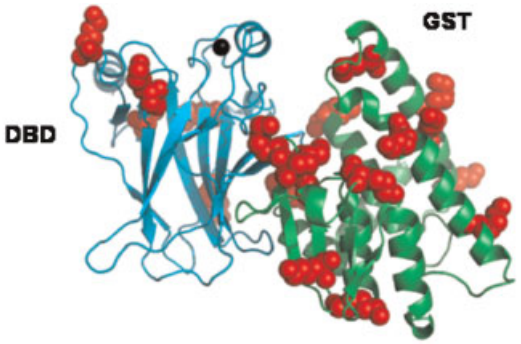

Figure 5. Three-dimensional structure of the best docking model for the DBD complex formed by the DBD domain of p53 and GST. Lysine residues are represented as red spheres.

complexes have been characterized by interfaces burying areas in the range between 900 and 1000 Å^2 (Jones and Thornton, 1996) and a predominance of non-polar residues at the interface. The model characterized by the highest solvent accessible surface area (SASA) together with a high percentage of non-polar residues at the interface, has been selected as the best complex. A graphical representation of this complex is given in Figure 5. Remarkably, the region of DBD which has been previously found to interact with AZ remains available for interactions with other molecules (De Grandis *et al*., 2007).

The selected DBD biomolecular system has been used to extract a model for the DBD-AZ complex. First, the 2000 complexes, generated by Zdock, have been first grouped by ClusPro by obtaining ten different models. These models have been then filtered in order to leave exposed the DNA binding domain of the DBD chain, by taking into account that the DBD-AZ complex has also to preserve the ability to bind DNA. A further filter has been applied to select only those models in which both the residues Met44 and Met64 of AZ are within a distance cut-off of 6 Å from the DBD. Such a requirement has been introduced to match the available experimental mutagenesis data on AZ, showing that both Met44 and Met64 of AZ are involved in the interaction with p53 (Yamada *et al*., 2002). Such a filtering process has reduced the number of candidate models to five groups. The physical properties of protein–protein interfaces for these five models are reported in Table 1. All the models are characterized by SASA values around 1000 Å^2, in a good agreement with what commonly detected for other complexes with strong character (Jones and Thornton, 1996; Nooren and Thornton, 2003). The

Table 1. Interface parameters for the five docking models of the DBD-AZ complex

Model (ClusPro ranking order)	SASA (Å^2)	Number of HB	DBD		AZ	
			% Polar atoms in interface	% Non-polar atoms in interface	% Polar atoms in interface	% Non-polar atoms in interface
1 (3)	721	4	38.6	61.4	51.3	48.7
2 (7)	956	9	44.9	55.0	31.6	68.3
3 (11)	493	4	46.5	53.8	59.3	40.7
4 (12)	852	4	43.9	56.1	55.7	44.3
5 (15)	548	8	36.7	63.3	45.4	54.6

SASA, solvent accessibility surface area; HB, hydrogen bond.

number of hydrogen bond (HB) established between the two proteins is between 4 and 9. In all models, we have found a dominance of non-polar residues at the interfaces, pointing out the presence of short-range hydrophobic interaction stabilizing the complex (Sheinerman *et al.*, 2000). Notably, the arrangement of the DBD with respect to AZ is closely similar to that of the best complex as extracted in our previous docking study between DBD and AZ without GST (De Grandis *et al.*, 2007). Additionally, no interaction of AZ with GST takes place, consistently with the experimental evidence that the presence of GST does not interfere with the interaction between DBD and AZ (Yamada *et al.*, 2002). Remarkably, Model n.2 is characterized by the highest SASA values and the highest number of HB, together with a high percentage of non-polar residues at the protein–protein interface. All these observations suggest that such a model could be the best complex for DBD-AZ. To provide further support to such a hypothesis, the extracted five models have been subjected to a further refinement by performing MD simulations in water. In such a way, possible structural changes arising from protein flexibility and solvation effects can be taken into account; the calculated interface parameters after the MD run being listed in Table 2, together with the time averaged root mean square displacement (RMSD) of the MD average structure from the X-ray structure. The fact that the RMSD values are in the range 4–5.5 Å for the five models, is indicative of slight reassessments of the structure upon the MD run. However, the interface parameters of these complexes are substantially stable after the MD run, with slight changes, generally indicative of a further stabilization of the complexes, as due to the relaxation of hydrated biomolecules. Notably, Model n.2 is still characterized by the best interface parameters and it has been chosen as our best complex for DBD-AZ; the graphical representation of this complex being given in Figure 6. At a visual inspection, the extracted model for the DBD-AZ appears to be very similar to the best complex previously extracted for the DBD (without GST) and AZ (De Grandis *et al.*, 2007). Such an observation is confirmed by the RMSD between these two models less than 0.4 nm and by the fact that the interface region between DBD and AZ of Model n.2, involves almost the same residues.

Comparison between the AFM and docking height distribution

By taking into account that each molecular structure can be anchored to the functionalized substrate through one of its available lysine residues, the predicted complexes can be found arranged in different ways on the substrate. This means that the anchored biomolecules can have different heights with respect to the substrate. To extract a distribution of the height for each complex, we have made the assumption that the higher the accessibility of a lysine, the more probable is its binding to the substrate. Accordingly, for each possible arrangement of the complex on the substrate, we have weighted the corresponding height with a factor given by the SASA of the anchoring lysine divided by the total accessibility of all the accessible lysine residues in the complex. The SASA values of lysine residues of DBD, before and after conjugation with AZ, are listed in Table 3. Generally, we note that lysine residues have a large SASA value, in agreement with the polar character favoring the exposition to the aqueous solvent. Furthermore, almost all the lysine residues in the biomolecule do not reveal significant changes in the SASA value upon the complex formation, consistently with the fact that they are generally not involved in the protein–protein interface regions (an exception being Lys139). Lysines with SASA values lower than 35 $Å^2$, expected to have a very low attachment probability, have not been taken into account.

The calculated distributions of the height for both the DBD and the DBD-AZ complexes are shown in Figure 7. In both cases, a single mode distribution with a significant spread in the height values was obtained. For DBD, the distribution is centered at 5.8 nm with a standard deviations of 2.1 nm, while for DBD-AZ, a

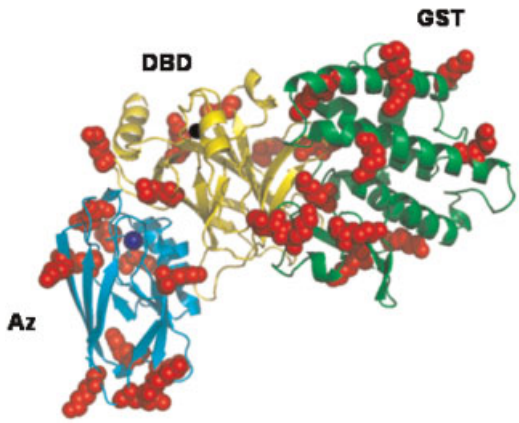

Figure 6. Three-dimensional structure of the best docking model for the DBD-AZ complex starting from the complex between DBD and GST (shown in Figure 5) and AZ. Lysine residues are represented as red spheres.

Table 2. Interface parameters for the five models of the DBD-AZ complex extracted from the docking, after a MD simulation run

Model (ClusPro ranking order)	RMSD (Å)	SASA ($Å^2$)	Number of HB	DBD		AZ	
				% Polar atoms in interface	% Non-polar atoms in interface	% Polar atoms in interface	% Non-polar atoms in interface
1 (3)	2.4	799	4	40.2	59.8	50.7	51.3
2 (7)	3.1	1011	9	40.5	59.5	34.5	65.5
3 (11)	3.8	542	4	42.5	57.5	56.3	43.7
4 (12)	2.3	899	4	44.1	55.9	53.7	46.3
5 (15)	2.6	589	8	38.7	61.3	48.2	51.8

RMSD, root mean square displacement; SASA, solvent accessibility surface area; HB, hydrogen bond.
The values are averaged over snapshots at 100 ps intervals during the last 1 ns of the MD simulation run.

Journal of Molecular Recognition

Table 3. Solvent accessibility surface area (SASA) of lysine residues of the DBD (formed by DBD domain and GST) before and after conjugation with AZ

Lysine residue number	SASA, DBD (Å^2)	SASA, DBD + AZ (Å^2)
2 (GST)	84	84
6 (GST)	15	15
23 (GST)	56	56
34 (GST)	55	55
35 (GST)	54	54
49 (GST)	100	100
93 (GST)	99	99
107 (GST)	108	108
122 (GST)	34	34
131 (GST)	139	139
132 (GST)	39	37
141 (GST)	115	115
169 (GST)	128	128
201 (GST)	133	133
101 (DBD)	150	150
120 (DBD)	128	117
132 (DBD)	11	11
139 (DBD)	89	44
164 (DBD)	95	95
Total	1548	1466

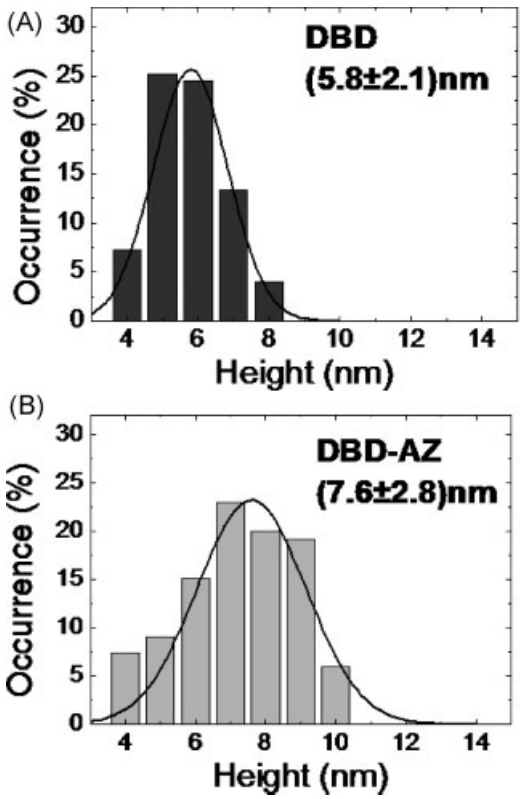

Figure 7. Histograms of the height for the docking models upon their anchoring onto a substrate through one of the available lysine residues: A) DBD and B) DBD-AZ DBD. Continuous lines: best-fit by a Gaussian distribution. The agreement between the histogram and the fitted Gaussian distributions has been checked by a χ^2-test at the confidence level of 90%.

central value of 7.6 nm and a standard deviations of 2.8 nm are estimated. In both the cases, the histograms can be well described by a single Gaussian, as checked by the χ^2 test (Figure 7 and the related legend). Notably, these height distributions find a good correspondence with those extracted by TM-AFM imaging (see Figures 2 and 3); such an agreement has been statistically verified by the *t*-test at a confidence level of 90%.

To further support the formation of a complex between DBD and AZ, we have estimated the volumes occupied by the DBD and DBD-AZ biomolecules by using the VolMap tool in the VMD software (Humphrey *et al*., 1996). We have found that the average volume passes from 320 nm^3 for DBD, to 450 nm^3 for DBD-AZ with an increase of about 40%. Such a change is statistically significant by assuming that the variability of the calculated volume is about 5%. Furthermore, this result finds a correspondence with the increase of 36% registered for the bearing volume analysis by TM-AFM images (see Figure 4). Accordingly, we can suggest that the measured increase in the bearing volume by adding AZ to DBD imaged spots, for DBD almost randomly arranged on the substrate, is consistent with the hypothesis that AZ interacts with DBD. Such a result, together with the previous data about the height distribution gets a further support for formation of a complex between DBD and AZ. In this respect, we would like to remark that the knowledge of the molecular structures of the systems, providing information on the topological properties of the systems, could help to interpret experimental data by AFM imaging.

CONCLUSION AND PERSPECTIVES

We have presented an approach which combines TM-AFM imaging to computational docking to describe the biorecognition complex between the DBD domain of p53 and the redox protein AZ. This complex deserves some interest for anticancer strategies. Starting from the known molecular structures of the DBD and AZ, we have first determined, by computational docking, the three-dimensional structure for their best complex. We have then developed a method to calculate the height distributions of the DBD domain when anchored to a functionalized gold substrate, before and after the addition of AZ. The found good agreement between the computed distributions and the experimental ones obtained by TM-AFM imaging lends support to the formation of a complex between DBD and AZ.

Such a combined approach by TM-AFM imaging and computational docking appears to be a rewarding tool to investigate in details the topological properties of a biomolecular structure immobilized on a substrate and to test, with a high sensitivity, the formation of complexes involving two, or even more, biomolecules. Furthermore, such a method could be suitable to complement force spectroscopy unbinding experiments between ligand-receptor pairs. Indeed, information on the topological properties of one of the partners (ligand or receptor) immobilized on the substrate could be of some help to extract kinetics information on the biorecognition process.

Acknowledgements

Thanks are due to Dr. Ada Sacchi for useful discussions and suggestions. L.A. acknowledges the Research Grant MUR "Brain Gain Project." This work has been partially supported by two PRIN-MIUR 2006 projects (no. 2006027587 and no. 2006028219).

REFERENCES

Bayburt TH, Sligar SG. 2002. Single-molecule height measurements on microsomal cytochrome P450 in nanometer-scale phospholipid bilayer disks. *Proc. Natl. Acad. Sci. USA* **99**: 6725–6730.

Berendsen HJC, Postma JPM, van Gunsteren WF, Hermans J. 1969. Interaction models for water in relation to protein hydration. *Nature* **224**: 175–177.

Bergkvist M, Carlsson J, Oscarsson S. 2001. A method for studying protein orientation with atomic force microscopy using relative protein volumes. *J. Phys. Chem. B* **105**: 2062–2069.

Bizzarri AR, Bonanni B, Costantini G, Cannistraro S. 2003. A combined study by AFM and MD simulation of a plastocyanin mutant chemisorbed on a gold surface. *Chem. Phys. Chem.* **4**: 1189–1195.

Bizzarri AR. 2006. Topological and dynamical properties of Azurin anchored to a gold substrate as investigated by molecular dynamics simulation. *Biophys. Chem.* **122**: 206–214.

Bizzarri AR, Brunori E, Bonanni B, Cannistraro S. 2007. Docking and molecular dynamics simulation of the azurin-cytochrome c551 electron transfer complex. *J. Mol. Recognit.* **20**: 122–131.

Bonander N, Leckner J, Guo H, Karlsson BG, Sjölin L. 2000. Crystal structure of the disulfide bond-deficient azurin mutant C3A/C26A. How important is the S-S bond for folding and stability? *Eur. J. Biochem.* **267**: 4511–4519.

Bonanni B, Kamruzzahan ASM, Bizzarri AR, Rankl C, Gruber HJ, Hinterdorfer P, Cannistraro S. 2005. Single molecule recognition between cytochrome C 551 and gold-immobilized azurin by force spectroscopy. *Biophys. J.* **89**: 2783–2791.

Bonanni B, Cannistraro S. 2005. Nanoparticles on modified glass surface as height calibration standard for atomic force microscopy operating in contact and tapping mode. *J. Nanotechnol.* **a0106**: 1–14.

Bonanni B, Bizzarri AR, Cannistraro S. 2006. Optimized biorecognition of cytochrome *c* 551 and azurin immobilized on thiol-terminated monolayers assembled on Au(111) substrates. *J. Phys. Chem. B* **110**: 14574–14580.

Bonanni B, Andolfi L, Bizzarri AR, Cannistraro S. 2007. Functional metalloproteins integrated with conductive substrates: detecting single molecules and sensing individual recognition events. *J. Phys. Chem. B* **111**: 5062–5075.

Butt HJ, Cappella B, Kappl M. 2005. Force measurements with the atomic force microscope: technique, interpretation, and applications. *Surf. Sci. Rep.* **59**: 1–152.

Calumet N, Simonson T. 2006. CysxHisy-Zn^{2+} interactions: possibilities and limitations of a simple pairwise force field. *J. Mol. Graph. Model.* **24**: 404–411.

Chen R, Weng Z. 2002. Docking unbound proteins using shape complementarity, desolvation, and electrostatics. *Proteins: Struct. Funct. Genet.* **47**: 281–294.

Chen R, Weng Z. 2003. A novel shape complementarity scoring function for protein-protein docking. *Proteins: Struct. Funct. Genet.* **51**: 397–408.

Cho Y, Gorina S, Jeffrey PD, Pavletich NP. 1994. Crystal structure of a p53 tumor suppressor-DNA complex: understanding tumorigenic mutations. *Science* **265**: 346–355.

Comeau SR, Gatchell DW, Vajda S, Camacho CJ. 2004. ClusPro: a fully automated algorithm for protein–protein docking. *Nucleic Acid Res.* **32**: 96–99.

Davis JJ, Hill HAO. 2002. The scanning probe microscopy of metalloproteins and metalloenzymes. *Chem. Commun.* **1**: 393–401.

De Grandis V, Bizzarri AR, Cannistraro S. 2007. Docking study and free energy simulation of the complex between p53 DNA-binding domain and Azurin. *J. Mol. Recognit.* **20**: 215–226.

Di Agostino S, Strano S, Emiliozzi V, Zerbini V, Mottolese M, Sacchi A, Blandino G, Piaggio G. 2006. Gain of function of mutant p53: the mutant p53/NF-Y protein complex reveals an aberrant transcriptional mechanism of cell cycle regulation. *Cancer Cell* **10**: 191–202.

Duan J, Nilsson L. 2006. Effect of Zn^{2+} on DNA recognition and stability of the p53 DNA-binding domain. *Biochemistry* **45**: 7483–7492.

Ferreira AAP, Colli W, Alves MJM, Oliveira DR, Costa PI, Güell AG, Sanz F, Benedetti AV, Yamanaka H. 2006. Investigation of the interaction between Tc 85-11 protein and antibody anti-T cruz by AFM and amperometric measurements. *Electrochim. Acta* **51**: 5046–5052.

Goto M, Yamada T, Kimbara K, Horner J, Newcomb M, Das Gupta TK, Chakrabarty AM. 2003. Induction of apoptosis in macrophages by *Pseudomonas aeruginosa* Azurin: tumour-suppressor protein p53 and reactive oxygen species, but not redox activity, as critical elements in cytotoxicity. *Mol. Microbiol.* **47**: 549–559.

Guex N, Peitsch MC. 1997. SWISS-MODEL and the Swiss-PdbViewer: an environment for comparative protein modelling. *Electrophoresis* **18**: 2714–2723.

Hess B, Bekker H, Berendsen HJC, Fraaije JGM. 1997. LINCS: a linear constraint solver for molecular simulations. *J. Comp. Chem.* **18**: 1463–1472.

Hoerber JK, Miles MJ. 2003. Molecular recognition imaging and force spectroscopy of single biomolecules. *Science* **302**: 1002–1005.

Horcas I, Fernandez R, Gomez-Rodriguez JM, Colchero J, Gomez-Herrero J, Baro AM. 2007. WSXM: a software for scanning probe microscopy and a tool for nanotechnology. *Rev. Sci. Instrum.* **78**: 013705–0137210.

Humphrey W, Dalke A, Schulten K. 1996. VMD – visual molecular dynamics. *J. Mol. Graph.* **14**: 33–38.

Jena JP, Hoerner JK. 2002. Atomic Force Microscopy in Cell Biology, Methods in Cell Biology, Vol. **68**, Academic Press: San Diego.

Joerger AC, Ang HC, Fersht AR. 2006. Structural basis for understanding oncogenic p53 mutations and designing rescue drugs. *Proc. Natl. Acad. Sci. USA* **103**: 15056–15061.

Jones S, Thornton JM. 1996. Principles of protein-protein interactions derived from structural studies. *Proc. Natl. Acad. Sci. USA* **93**: 13–20.

Kholmurodov K, Smith W, Yasuoka K, Darden T, Ebisuzaki T. 2000. A smooth-particle mesh Ewald method for DL_POLY molecular dynamics simulation package on the Fujitsu VPP700. *J. Comput. Chem.* **21**: 1187–1191.

Kim KY. 2007. Nanotechnology platforms and physiological challenges for cancer therapeutics. *Nanomed. Nanotechnol. Biol. Med.* **3**: 103–110.

Levine AJ. 1997. p53, the cellular gatekeeper for growth and division. *Cell* **88**: 323–331.

Maynard AT, Covell DG. 2001. Reactivity of zinc finger cores: analysis of protein packing and electrostatic screening. *J. Am. Chem. Soc.* **123**: 1047–1058.

Nar H, Messerschmidt A, Huber R, van de Kamp M, Canters GW. 1991. Crystal structure analysis of oxidized Pseudomonas aeruginosa Azurin at pH 5.5 and pH 9.0. *J. Mol. Biol.* **221**: 765–772.

Nie S, Xing Y, Kim GJ, Simons JW. 2007. Nanotechnology applications in cancer. *Annu. Rev. Biomed. Eng.* **9**: 257–261.

Nishida M, Harada S, Noguchi S, Satow Y, Inoue H, Takahashi K. 1998. Three-dimensional structure of Escherichia coli glutathione S-transferase complexed with glutathione sulfonate: catalytic roles of Cys10 and His106. *J. Mol. Biol.* **281**: 135–147.

Nooren IMA, Thornton JM. 2003. Structural characterization and functional significance of transient protein-protein interactions. *J. Mol. Biol.* **325**: 991–1018.

Nose' S. 1984. A molecular dynamics method for simulations in the canonical ensemble. *Mol. Phys.* **52**: 255–268.

Parrinello M, Rahman A. 1981. Polymorphic transitions in single crystals: a new molecular dynamics method. *J. Appl. Phys.* **52**: 7182–7190.

Rief M, Grubmueller H. 2002. Force spectroscopy of single biomolecules. *ChemPhysChem.* **3**: 255–261.

Schitter G, Stark RW, Stemmer A. 2004. Fast contact-mode atomic force microscopy on biological specimen by model-based control. *Ultramicroscopy* **100**: 253–257.

Sengupta S, Sasisekharan R. 2007. Exploiting nanotechnology to target cancer. *Br. J. Cancer* **96**: 1315–1319.

Sheinerman FB, Norel R, Honig B. 2000. Electrostatic aspects of protein-protein interactions. *Curr. Opin. Struct. Biol.* **10**: 153–159.

Spieger MR. 1961. Statistics. McGraw-Hill Book Company: New York.

Stolz M, Aebi U, Stoffler D. 2007. Developing scanning probe-based nanodevices – stepping out of the laboratory into the clinic. *Nanomed. Nanotechnol. Biol. Med.* **3**: 53–62.

Taranta M, Bizzarri AR, Cannistraro S. 2008. Probing the interaction between p53 and the bacterial protein azurin by single molecule force spectroscopy. *J. Mol. Recognit.* **21**: 63–70.

Vajda S, Camacho CJ. 2004. Protein – protein docking: is the glass half-full or half-empty? *Trends Biotechnol.* **22**: 110–116.

van de Kamp M, Silvestrini MC, Brunori M, Beeumen JV, Hali FC, Canters GW. 1990. Involvement of the hydrophobic patch of azurin in the electron-transfer reactions with cytochrome 551 and nitrite reductase. *Eur. J. Biochem.* **194**: 109–118.

van der Spoel D, van Buuren AR, Apol E, Meulenhoff PJ, Tieleman DP, Sijbers A, Hess B, Feenstra KA, Lindahl E, van Drunen R, Berendsen HJC. 2001. GROMACS User Manual (University of Groningen, Groningen, The Netherlands), Version 3.2.

Vogelstein B, Lane DP, Levine AJ. 2000. Surfing the p53 network. *Nature* **408**: 307–310.

Yamada T, Goto M, Punj V, Zaborina O, Chen ML, Kimbara K, Majumdar D, Cunningham E, Das Gupta TK, Chakrabarty AM. 2002. Bacterial redox protein Azurin, tumor suppressor protein p53, and regression of cancer. *Proc. Natl. Acad. Sci. USA* **99**: 14098–14103.

Yamada T, Hiraoka Y, Ikehata M, Kimbara K, Avner BS, Das Gupta TK, Chakrabarty AM. 2004. Apoptosis or growth arrest: modulation of tumor suppressor p53's specificity by bacterial redox protein Azurin. *Proc. Natl. Acad. Sci. USA* **101**: 4770–4775.

Zhao J, Davis JJ, Sansom MSP, Hung A. 2004. Exploring the electronic and mechanical properties of protein using conducting atomic force microscopy. *J. Am. Chem. Soc.* **126**: 5601–5609.

